 doi:10.20944/preprints202011.0340.v1

Type of the Paper (Article)

Analysis of Impact Characteristics and Detection of Internal Defects for Unidirectional Carbon Composites with Respect to Fiber Orientation

Sun-ho Go[1], Alexandre Tugirumubano[2], and Hong-gun Kim[2,3,#]

[1] Mechanical Testing Center, ITEL Co., LTD.; sh.go@itel.re.kr (S.H.G)
[2] Institute of Carbon Technology, Jeonju University; alexat2020@jj.ac.kr(A.T)
[3] Department of Mechanical and Automotive Engineering, Jeonju University; hkim@jj.ac.kr (H.G.K)
* Correspondence: hkim@jj.ac.kr; Tel.: +82-63-220-2613

Abstract: With the increasing use of carbon fiber reinforced plastics in various area, carbon fiber composites based on prepregs have attracted attention in industries and academia research. However, prepreg manufacturing processes are costly, and the strength of structures varies depending on the orientation and defects (pores and delamination). For non-contact evaluation of internal defects, we proposed lock-in infrared thermography to investigate orientation angles after a compression test. We also conducted a drop-weight impact test to study the behaviour of the composites after impact according the fibers orientation for composite fabricated using unidirectional carbon fiber prepregs. Using CAI tests, we determined the residual compressive strength and confirmed the damage modes using a thermal camera. The results of the drop weight impact tests show that the specimen laminated at 0° suffered the largest damage because of susceptibility of the resin to impact. In contrast, the specimens oriented in of 0°/90° and +45°/–45° directions transferred more than 90% of the impact energy back to the impactor because of the lamination of fibers in the orthogonal directions. Furthermore, the specimens that underwent complete damage in the impact tests were subjected to the lock-in method and showed internal delamination and cut fibers. With the finite elements analysis, the damage of each ply could be observed. Moreover, the temperature differences in the residual compression tests were not significant.

.

Keywords: drop-weight impact; unidirectional carbon composites; orientation angle; internal defect; impact

1. Introduction

In recent years, the industrial application of composite materials has rapidly expanded with the aim of decreasing in energy consumption and the development of new materials with lightweight characteristic. Among them, carbon fiber-reinforced plastics (CFRPs) have been used in several industries that require weight reduction, due to their higher specific strength and higher specific stiffness and low density, their excellent chemical resistance and electrical properties when compared with existing metallic materials [1-3]. The CFRPs are the composites where the carbon fibers are used as strengthening elements to provide high strength in polymer matrix. The long carbon fibers are the most used to fabricate the composites for structural applications. The common method of fabricating these composites is through laminating the dry carbon fibers fabrics by using polymer as binding element or laying up the carbon fibers fabrics pre-impregnated with resin (prepreg). The carbon fiber fabrics may be either unidirectional (UD) or woven. Unlike the woven carbon fiber fabrics that have

 doi:10.20944/preprints202011.0340.v1

large gaps between the fibers due the interlacing of the yarns (warp and wefts), in the unidirectional carbon fiber fabrics, the gaps are almost absent because the fibers are tightly assembled in single and parallel direction [4]. The properties of the CFRP depend on the lamination sequence, orientation of the fibers and manufacturing methods.

Due to the development of three-dimensional automatic fiber placement technologies, carbon composites with prepregs have attracted significant research attention. However, the processes that involves prepregs are costly, and the strength varies significantly depending on the fiber orientation and defects, such as delamination and pores. Those defects can degrade the quality and the performance of the composites. The production of good quality composites involves the experience, suitable manufacturing process and quality testing. Hence, a non-destructive evaluation method is of urgent need to investigate the quality of the produced composites [5,6].

Among the existing non-destructive evaluation methods for CFRPs, defect imaging based on ultrasonic C-scans has been effectively employed [2]. Given that the method is a contact type, there are size and process limitations. The infrared (IR) thermography using IR thermal imaging cameras allows for the determination of the surface temperature distribution of an object based on IR waves emitted from the surface, and has been extensively implemented in non-contact temperature measuring equipment [7]. Infrared thermography involves the detection of radiant energy from the surface of an object, and its conversion into the temperature domain, thus revealing the thermal distribution in a real-time image. However, defect detection for objects with high thermal diffusion coefficients is challenging, and can be realized by the application of the lock-in method [3,7].

The detection mechanism of the lock-in system is based on the synchronization of the heat source signal with the noise from an IR thermal imaging camera that measures the IR radiation generated from the surface of a specimen under periodic loading. The differences between the heat source signal and response signal of the object are then obtained and analyzed.

In particular, given that CFRPs are susceptible to impacts, research on the improvement of their impact performance is required. It is common knowledge that the damage due to the impact of composite materials varies with respect to the impact velocity, and that local impact damage can be attributed to the insufficient impact response time of composite materials at low impact speeds of 1–100 m/s, and high impact speeds [8-12]. In the case of low-speed impacts, non-visible microscopic damage mainly occurs due to impact. In addition, given the high elasticity of CFRPs, the kinetic energy of the impactor is stored in the CFRP as absorbed energy under low-speed impacts, and it is then re-transferred to the kinetic energy in the impactor through elastic restoration [8, 13-22].

This work aims to study the mechanical impact performance of the CFRP through the drop-weight impact testing according to the orientation of the unidirectional carbon fiber fabrics. Further, the non-destructive inspections of the defects caused by impact test were performed using lock-in infrared thermography method. In addition, the finite element analysis was conducted to investigate the damage behavior of each ply in the composites and compared the damage geometry of the analysis with that of non-destructive test. The compression after impact test was also conducted to evaluate the residual compressive strength of the composites. Besides, to assess the temperature variation at the failure of the composites during the testing, the infrared camera was used.

2. 2. Materials and Method

2.1 Material and Composite Manufacturing

The material used in this study was UIN200C which is a unidirectional carbon fiber prepreg purchased from SK Chemical, Korea. The laminated prepreg was manufactured using the autoclave molding process, as shown in Figure 1(a). Figure 1(b) presents the molding process, and Table 1 presents the physical properties of the material. The following three composites with different orientation angles were fabricated: a composite with a 34-plies unidirectional prepreg at 0°, a composite with a 34-ply prepreg cross-laminated at 0°/90°, and a composite with a 34-ply prepreg cross-laminated at +45°/–45°. For each lamination configuration, the plate specimen with dimensions

Preprints (www.preprints.org) | NOT PEER-REVIEWED | Posted: 12 November 2020 doi:10.20944/preprints202011.0340.v1

of 450 mm × 420 mm were fabricated. Four specimens for each composite were tested to evaluate the impact and compression after impact behavior of the composites.

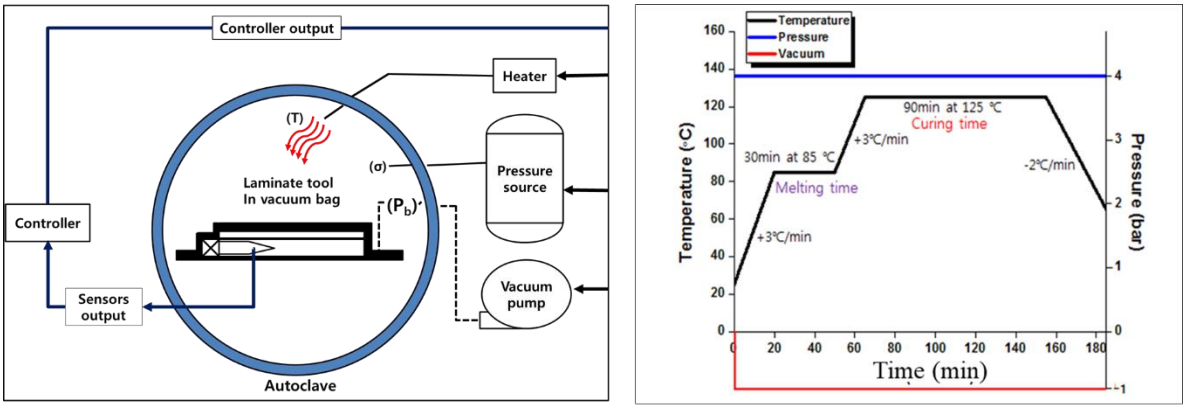

(a) (b)

Figure 1. Molding Process; (a) Flow Diagram of Autoclave Molding Method and (b) Molding process conditions

Table 1. Physical properties of UIN200C material

Thickness (mm)	Fiber Areal Wt. (g/m²)	Resin Content (%)	Total Wt. (g/m²)
0.18	200	30	448

2.2 Drop-Weight Impact Test

The drop-weight impact test was conducted for the fabricated composites. In previous studies, the drop-weight impact failure trend of polymer materials has been found to occur through either the matrix cracking damage of the single layer, which is internal damage; or delamination from the interface; or the external damage. Thus, there exist three cases of failure mode in composite due to drop-weight impact [13, 21, 23]. In the case of the puncture failure mode (P-mode), the full-penetration failure geometry can be observed, in which the diameter of the failure site is almost equal to that of the weight. This failure behavior can be observed in polycarbonate and polyethylene. In the case of the crack failure mode (C-mode), a failure is generated at the deformation zone around the weight collision site, and cracks are propagated toward the surrounding areas. The failure mode can be observed in polypropylene and propylene-ethylene block co-polymers. In the case of the brittle fracture mode (B-mode), a failure occurs with radial crack propagation from the center of the specimen. Moreover, this failure behavior is observed in polystyrene, and the brittle failure mode has a slight influence on the absorption energy [13, 15-17, 23].

In this study, for the drop-weight impact test, the test conditions and specimen specifications were selected in accordance with the ASTM D 7136 standard, and the analysis was conducted for three specimens per type of composite. The impact absorption efficiency, e_{abs}, of each material was analyzed using the following equation (1):

$$e_{abs}(\%) = \frac{J_a}{J_i} \times 100 \quad (1)$$

 doi:10.20944/preprints202011.0340.v1

Where J_i and J_a are the impact energy (in Joule) and the impact absorption energy (in Joule), respectively, which were obtained from the drop-weight impact test results, for a comparison of their impact absorption performances under the same impact energy conditions. In addition, a IR thermal image camera was used for the conversion of the radiant energy generated during impact into the temperature domain, and for the analysis of the relationship between the impact energy and heat energy. In addition, the mode that leads to failure was determined based on the thermal distribution of the impact energy flow. Given that the weight, speed, and drop height are critical parameters in the drop-weight impact test, they were calculated and applied using the formulas specified in the standard. The weight used was 4.23 kg, and the test was conducted with a drop height of 0.92 m and a drop speed of 4.21 m/s. Figure 2 presents the test equipment and components used. The temperature results were compared and analyzed by determining the difference between the room temperature before the test and the maximum temperature during breakage (ΔT).

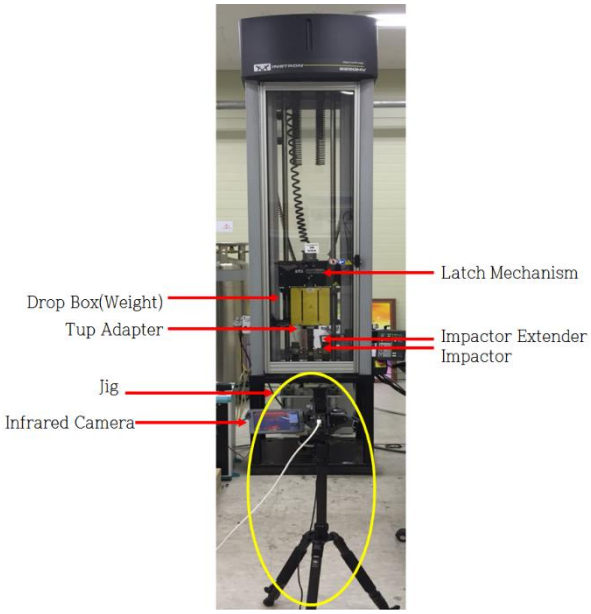

Figure 2. Experimental setup

2.3 Compression-after-impact Test

The compression test conducted on the specimen that underwent into impact test is mainly referred to as the compression-after-impact (CAI) test. The CAI was conducted in accordance with the ASTM D 7137 standard. It is the common knowledge that the CAI test is conducted for examining the matrix cracking and fiber breakage after impact damage with respect to the lateral shear and vertical stress of laminated composites, in addition to the compressive strength after impact [24-27]. In particular, delamination is known to reduce the compressive strength of laminated composites by 40%–60%. The CAI strength was calculated based on the compressive load and cross-sectional area of the specimen, using the installed jig, as shown in Figure 3. In the test, the IR thermal image camera was also used to identify the temperature distribution with respect to breakage. The temperature results were then compared and analyzed based on the difference between the room temperature and the maximum temperature during breakage (ΔT). In addition, the strength degradation after impact was compared with the compressive strength of WSN-3K, which was approximately 438.77 MPa, as obtained from previous studies.

Preprints (www.preprints.org) | NOT PEER-REVIEWED | Posted: 12 November 2020 doi:10.20944/preprints202011.0340.v1

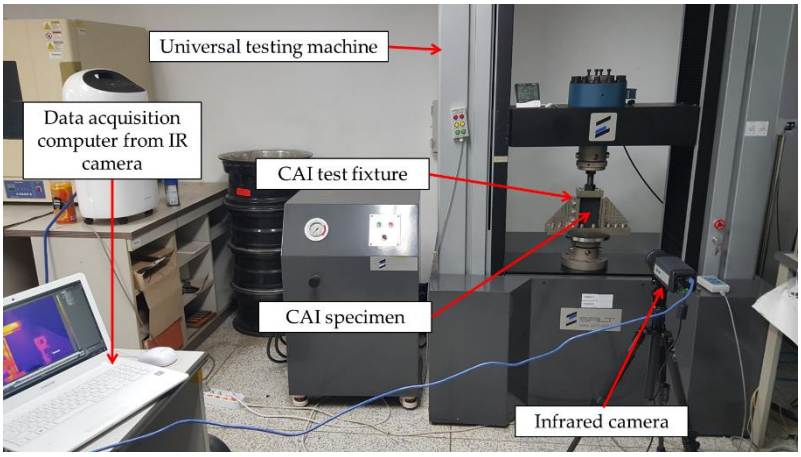

Figure 3. CAI experimental setup

2.4 Lock-In Thermography

The lock-in method considered in this study for non-destructive inspection (Figure 4), which is referred to as lock-in IR thermography, was employed to obtain the response signal of the object by synchronizing a halogen lamp (heat source) with the IR detection element of the thermal imaging camera, and to realize the detection based on the changes in the infiltrated heat source signal. In this case, the one-dimensional heat conduction equation (2) in the solid was used as follows [7,14]:

$$\frac{\partial T}{\partial t} = \frac{k}{\rho C_p}\frac{\partial^2 T}{\partial x^2} \quad (2)$$

In Equation (1), T is the temperature, t is the time, k is the thermal conductivity, ρ is the density, C_p is the specific heat, and x is the distance in the heat flow direction. The solution of Equation (2) based on the harmonic function can be expressed as Equation (3) [7]:

$$T(x,t) = T_o e^{-x/\mu}\cos\left(\omega t - \frac{x}{\mu}\right) \quad (3)$$

Where μ is the thermal diffusivity and T_o is the initial temperature.

The lock-in method can improve the detection sensitivity by extracting the phase from the measurement results using Equation (3), and minimize the defect detection error due to the non-uniformity of the surface emissivity. The phase in Equation (3) can obtain IR detection signals S_1, S_2, S_3, *and* S_4, which are consecutive at the intervals of the $\lambda/4$ period of the heat source, by synchronizing the external heat source with the IR detection element. Finally, the results can then be obtained using Equations (5) and (6) [7]:

$$\begin{aligned} S_1 &= T_o e^{-x/\mu}\cos\left(\omega t - \frac{x}{\mu}\right) \\ S_2 &= T_o e^{-x/\mu}\cos\left(\omega t - \frac{x}{\mu} - \frac{\pi}{3}\right) \\ S_3 &= T_o e^{-x/\mu}\cos\left(\omega t - \frac{x}{\mu} - \pi\right) \\ S_4 &= T_o e^{-x/\mu}\cos\left(\omega t - \frac{x}{\mu} - \frac{3\pi}{2}\right) \end{aligned} \quad (5)$$

Preprints (www.preprints.org) | NOT PEER-REVIEWED | Posted: 12 November 2020 doi:10.20944/preprints202011.0340.v1

$$\emptyset = \frac{x}{\mu} = tan^{-1}\left(\frac{S_4 - S_2}{S_1 - S_3}\right) \quad (6)$$

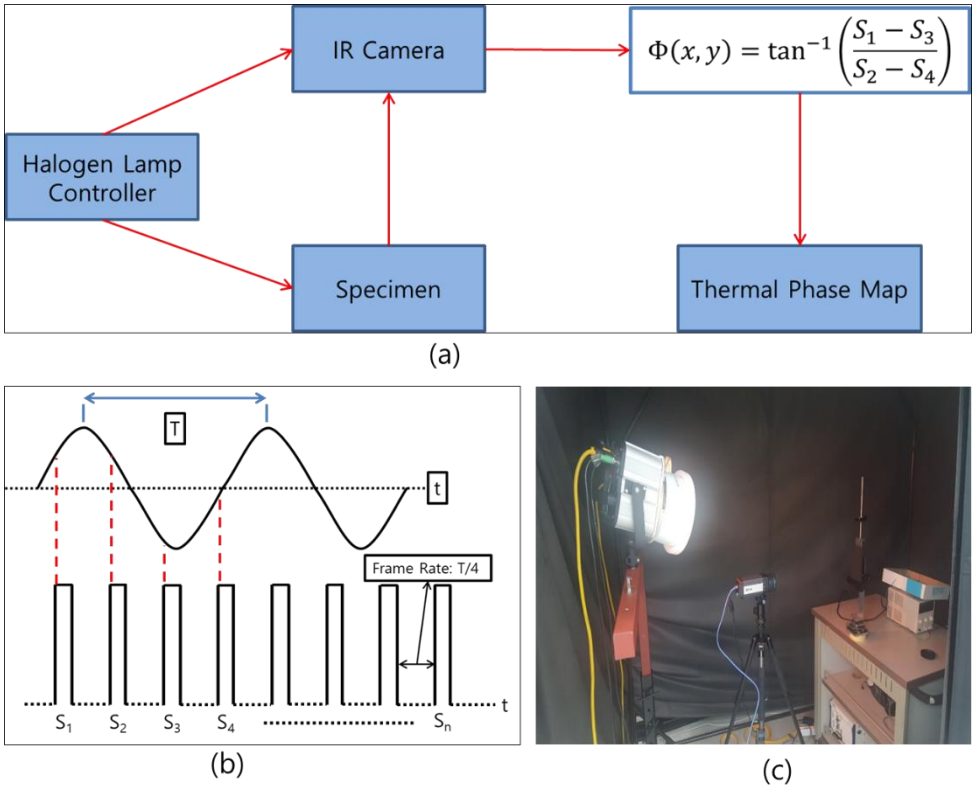

Figure 4. Lock-in Method: (a) Flowchart; (b) Diagram and (c) Experimental Setup

2.5 Finite Element Analysis of Carbon Composite

The finite element analysis (FEA) was conducted to simulate the impact behavior of composites. The composites design and the analysis were performed using the ANSYS Composites Pre&Post Processor (ACP) which is a composite material stacking module in ANSYS. The composite model was defined as in the actual lamination stacking and the analysis was performed in the similar conditions as the testing conditions. For the uni-directional carbon composites, the tensile strength of 2653.04 MPa, tensile modulus of 162.58 GPa, Poisson's ratio of 0.33 and density of 1.49 kg/m3 were used as material properties for the analysis and the boundary conditions were defined in the same way as ASTM D7136. This analysis was done to evaluate the impact failure behavior of each ply and compare the failure image of the composites from the analysis with that of the actual drop tested specimen obtained using non-destructive test (lock-in thermography) results.

3. Results and Discussion

3.1 Results of Impact Test

The following results (Figure 5(a-b) and Table 2) were obtained for the composite in which the unidirectional prepregs were laminated at an angle of 0°. Given that the carbon fibers were laminated

 doi:10.20944/preprints202011.0340.v1

in one direction, the specimen underwent breakage in the direction of the carbon fiber after impact. The same conclusion could be obtained from the thermal distribution image. The impact absorption efficiency was 85%, which indicates that 85% of the applied impact was absorbed by the specimen. Practically, in the case of the carbon composite with lamination in 0° direction, the epoxy support was in the transverse direction, and not in longitudinal direction (the fiber direction). Moreover, due to the brittleness of the resin, breakage of the matrix has easily occurred.

Table 2. Impact Test Results for Specimens Laminated in 0° Direction

#	Max. Load (kN)	Total Energy (J)	Impact Energy (J)	Efficiency (%)	Temperature (°)
1	5.00	33.59	37.74	89.0%	34.92
2	4.94	28.52	37.37	76.3%	38.35
3	4.69	28.91	37.19	77.7%	54.88
4	4.82	31.94	37.56	85.0%	55.94
Avg.	4.86	30.74	37.47	82.0%	46.02

Figure 5 (c-d) and Table 3 present the test results for the composite in which carbon fibers were cross-laminated at an angle of +45°/–45°. A different trend from that of the composite laminated in one direction was observed (Figure 5c). The impact absorption efficiency was 7.9% on average, which indicates that the applied impact applied was re-transferred to the impactor. The thermal image (Figure 5d) shows the cracks generated during the transmission of the impact load from the impact site across the composites. The results showed that the cracks tended to propagated in the similar direction as the fiber orientation. This means that the damages were mainly due to breakage of brittle epoxy matrix which caused the progressive debonding (separation) of the adjacent fibers close to the impact site in the fiber orientation.

Table 3. Impact Test Results for Specimens Laminated in +45°/–45° Direction

#	Max. Load (kN)	Total Energy (J)	Impact Energy (J)	Efficiency (%)	Temperature (°)
1	10.92	1.87	37.72	5.0%	3.96
2	10.52	2.80	37.33	7.5%	3.61
3	10.37	3.06	37.25	8.2%	3.36
4	10.39	4.12	37.78	10.9%	3.58
Avg.	10.55	2.96	37.52	7.9%	3.63

Figure 5 (d-f) and Table 4 present the test results of the composite in which carbon fibers were cross-laminated in 0°/90° orientation. As for the composites with +45°/–45° orientation, Figure 5d showed different trend from that of the composite laminated in one direction was observed (Figure 5a). The average impact absorption efficiency was -1.3%, which indicates that the applied impact was re-transferred to the impactor. The thermal distribution image reveals the generation of cracks during the transmission of the impact loading from the impact site through the thickness of the composites. Different from the other configurations, it could be seen that the propagation of cracks due to the impact test were in two orthogonal directions with long and extended crack propagation in direction perpendicular to the fiber's orientation. However, from the thermal image (Figure 5d), it can be seen that the very critical damages occurred in the vertical direction (fiber orientation) which can be

 doi:10.20944/preprints202011.0340.v1

attributed to breakage of both matrix and fibers. Figure 5(b,d,f) showed that at the impact site, the damage were severe. That can be associated to the fracture of fiber and matrix at that location on the side of the impactor, and the other damages such as the push-out delamination [5] due to the transmission of impact load through the composites around the impact location.

Table 4. Impact Test Results for Specimens Laminated in 0°/90° Direction

#	Max. Load (kN)	Total Energy (J)	Impact Energy (J)	Efficiency (%)	Temperature (°)
1	12.26	–0.45	37.80	–1.2%	3.27
2	12.35	–0.93	37.47	–2.5%	2.98
3	12.25	–0.28	37.54	–0.7%	4.50
4	12.09	–0.26	37.42	–0.7%	4.30
Avg.	12.24	–0.48	37.56	–1.3%	4.01

Preprints (www.preprints.org) | NOT PEER-REVIEWED | Posted: 12 November 2020 doi:10.20944/preprints202011.0340.v1

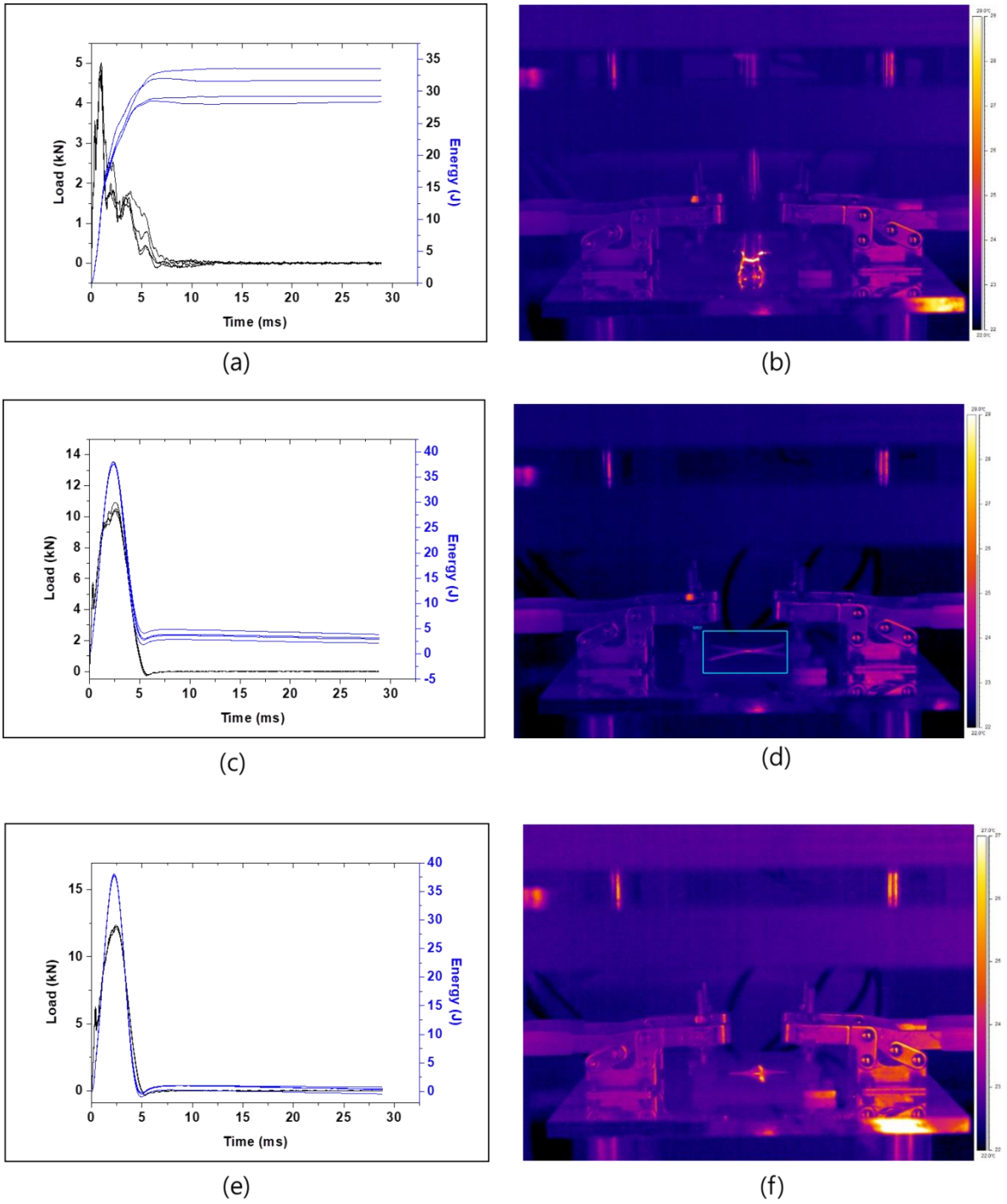

Figure 5. Impact Test Results for Energy and Load of Specimens with Respect to Time (Left), and Thermal Distribution Image (Right): (a)-(b) Specimen Laminated at an Angle of 0º; (c)-(d) Specimen Laminated at an Angle of +45°/–45° and (e)-(f) Specimen Laminated at an Angle of 0°/90°

3.2 The FEA and Thermography Results

Figure 6 presents the images of the analyzed specimens after the drop-weight impact test using the lock-in method for the specimens +45°/–45° and 0°/90°. In the case of the specimen laminated at angle of 0°, the non-destructive inspection method was not conducted due to the fact that the composite with all plies oriented in 0° was completely broken by the drop-weight impact test. The

 doi:10.20944/preprints202011.0340.v1

lock-in non-destructive test was performed to conform the internal damage of the test specimen after the actual drop-impact test.

The images on the left-hand side, in Figure 6, are the images of the specimens after impact, whereas those on the right-hand side are the images of the same specimens analyzed using the non-destructive inspection method. After the impact test, the mark left by the impactor and small cracks could be observed with naked eye to assess the degree of the external damage (Figure (a) and (c)). However, the internal damages could be observed by using the lock-in non-destructive test. It can be seen that the lock-in non-destructive technique, the extension of damage and the overall geometry of the damage in the composite could be detected. The geometry of damage depended on the stacking structure of the composites and in both, the long axes (or the diagonals) of the damage shapes were oriented in the same direction as the principal direction of laminated plies. This indicated that the damage propagation in the CFRP composites (with long fibers) mostly follows the fiber orientation. This behavior was believed to be associated with the progressive separation of carbon fibers along their directions due to the breakage of brittle epoxy matrix and the crack propagations from the impact location.

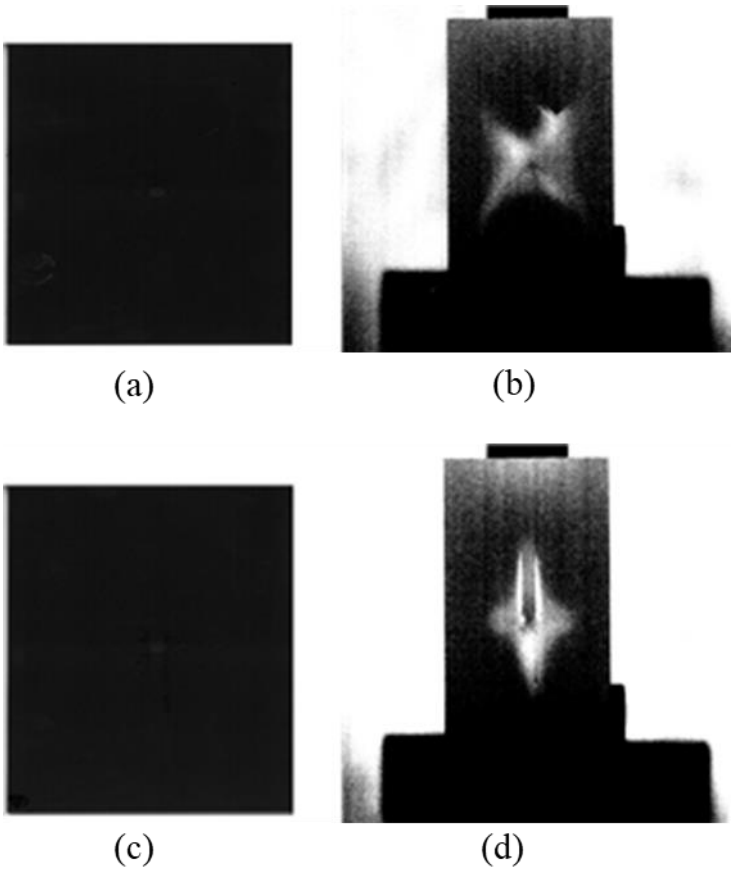

Figure 6. Digital Camera Images For External View (Left) and Lock-in Thermagraphy Image for Defects Detections (Right): (a-b) Specimen Lamination in +45°/–45° and (c-d) Specimen Lamination in 0°/90°

Figure 7 (a-b) show the FEA failure image in each and every ply for specimen laminated in in +45°/–45° and in 0/90°. It should be noted that, the impact loading was applied on the side of ply number 1 (P1) and transmitted through the thickness of the composites. The finite element analysis (FEA) results showed that the impact damage created by the impactor has ellipsoidal shape, with the long (principal) axis oriented in fiber direction of each plie, for the plies stacked

 doi:10.20944/preprints202011.0340.v1

in the first half of the composite from the impactor side. By considering pair by pair of plies (+45° ply and –45°ply), it can be seen that for +45°/–45° composite, every pair of plies had almost similar size of damages, except that the long axes of ellipsoidal damage in first ply is perpendicular to the one in second ply of pair. On the other hand, for 0°/90° composite, the comparison of (0°/90°) pair of plies showed that damage (ellipsoidal shape) which occurred in 0° ply had shorter long (principal) axis than the one which occurred in 90° ply. Those observation were in consistent of the principal axis of damages obtained using lock-in thermography. The FEA results also showed, in both composites, that from a pair of plies to following pair, the surface of critical damage (in red) around the impact location gradually decreased up to the middle pair of plies (P18 and P19) and then start to increase again toward the outer plies. It could be seen that in the second half of the composite laminations, the shape of damage was changed into a sum of about two small ellipsoidal damages with their long axis being perpendicular. This may indicate that, in the first half of composite lamination, the damage occurred, in each ply, mainly due to impactor, and the effect of impact load slowly decreased toward inside the composites. However, in the second half the damage in each ply occurred due to the composites impact load of the impactor and the impact load from the preceding ply. In ANSYS ACP, the typical failure image of damage in each ply could be acquired, but the image of damage of the whole model of composites could not be obtained to compare with the lock-in images. However, based on the shape and the orientation of the principal axis of the damage obtained with FEA, it could be inferred that the damage detected by using lock-in testing was the combination of the damage that occurred in each ply of the composites.

Preprints (www.preprints.org) | NOT PEER-REVIEWED | Posted: 12 November 2020 doi:10.20944/preprints202011.0340.v1

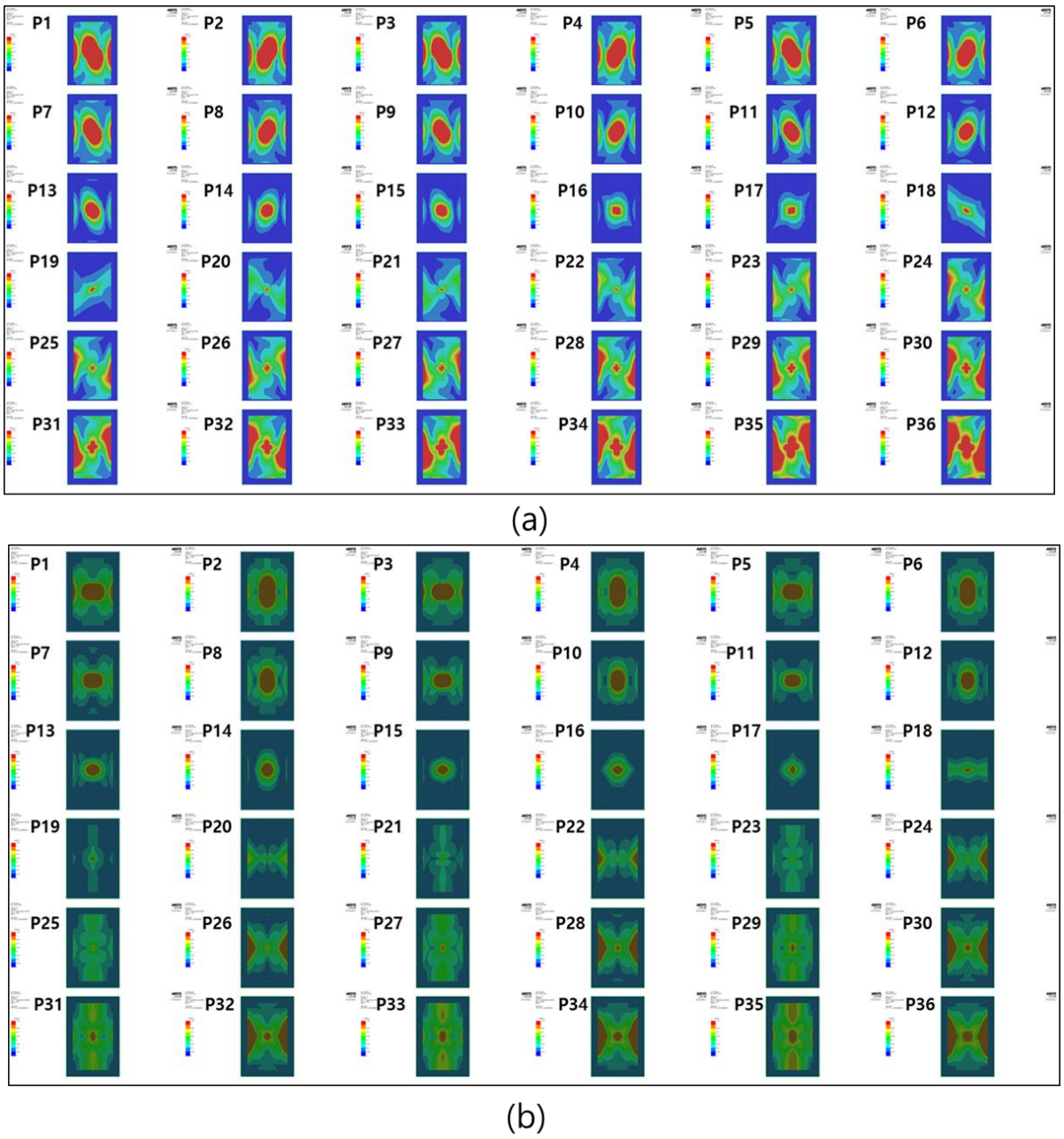

Figure 7 FEA images of the damage in each ply of the composites: (a) +45°/–45 and (b) 0°/90

3.3 Results of CAI Test

The CAI test results shown in Figure 8 (a-b) and Table 5 of the specimens laminated at angles of 0°/90° and +45°/–45°. The CAI test was not conducted on the specimen laminated at an angle of 0°, as it was completely destroyed by the drop-weight impact test. In the case of the specimen laminated at an angle of +45°/–45°, the residual compressive strength was 67.02 MPa, and the temperature difference was 2.56 °C, thus indicating a negligible temperature difference. This can be attributed to the lack of supporting fibers in the load direction, and the orientation of fibers at angles of ±45°.

In the case of the specimen laminated at an angle of 0°/90° (Figure 8(c-d) and Table 5), the residual compressive strength was 113.78 MPa and the temperature difference was 10.66 °C, which was slightly larger than those of the specimen laminated at an angle of +45°/-45°. However, the temperature variation was greater than the temperature difference due to the impact test. These results were obtained due to the prior breakage of the specimen. In addition, the thermal image confirmed that the cracks propagated in the orthogonal direction from the impact site for the composite with 0°/90° configuration.

Preprints (www.preprints.org) | NOT PEER-REVIEWED | Posted: 12 November 2020 doi:10.20944/preprints202011.0340.v1

Table 5. CAI Test Results of Specimen According to the Lamination Angle

Direction of Lamination	Specimens No	Area (mm^2)	Max Load (kN)	Residual Compressive Strength (MPa)	Temperature (°C)
+45°/-45°	1	540.73	37.56	69.46	4.48
	2	542.27	37.18	68.56	3.69
	3	540.73	36.58	67.65	3.41
	4	544.30	36.48	67.02	2.56
	Avg.	542.01	36.95	68.17	3.53
0°/90°	1	532.72	56.82	106.66	11.90
	2	538.46	54.32	100.88	8.94
	3	542.16	55.70	102.74	10.34
	4	537.35	61.14	113.78	10.66
	Avg.	537.67	57.00	106.01	10.46

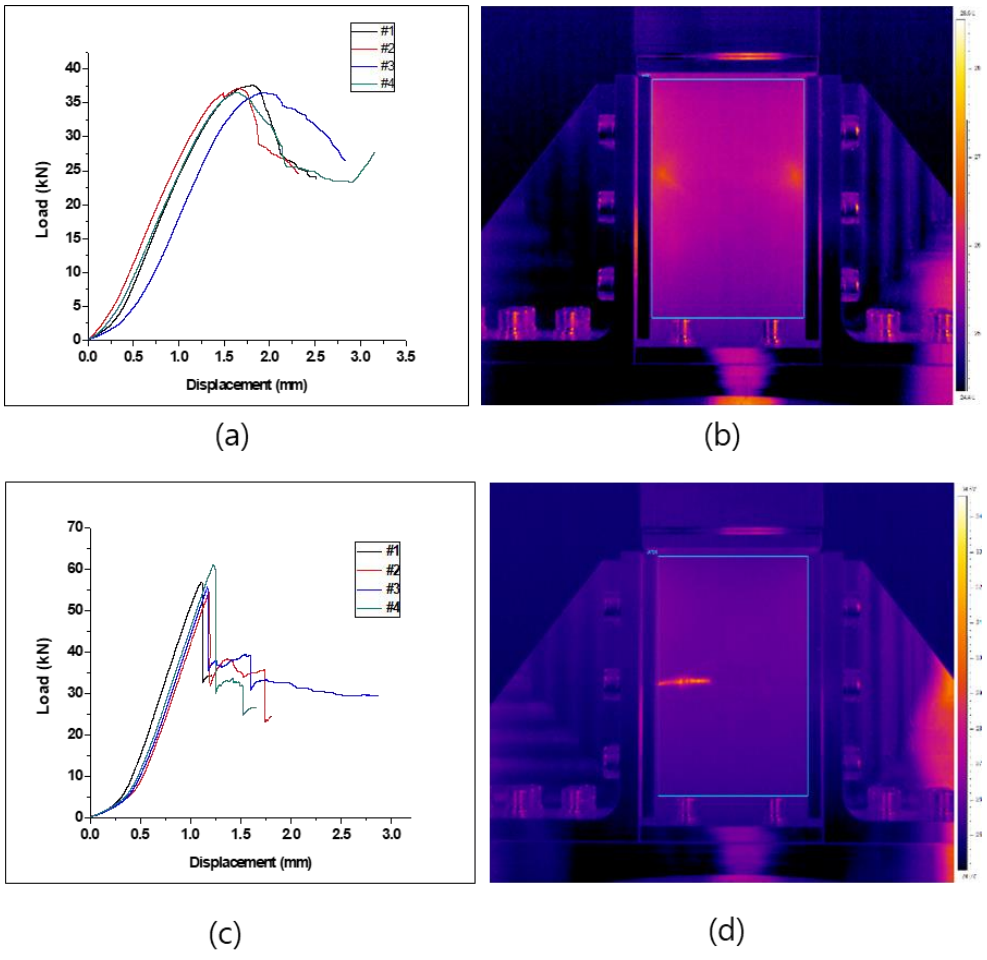

Figure 8. Load-Displacement Curve of the CAI Test (Left) and Thermal Image of CAI Test (Right): (a-b) Specimen Lamination in +45°/–45° and (c-d) Specimen Lamination in 0°/90°

4. Conclusions

Unidirectional carbon fiber prepregs were laminated at three orientation angles, i.e., 0°, 0°/90°, and +45°/–45°, and the drop-weight impact test was conducted. After impact, the internal damage of the specimens was examined using the lock-in method, which is a non-destructive inspection method. Thereafter, the residual compressive strength was determined from the CAI test results, and the damage modes were confirmed using the IR thermal image camera. The conclusions of this study can be summarized as follows.

The results of the drop-weight impact test on the carbon composites at three different orientation angles revealed that the specimen laminated at angle of 0° absorbed the most impact energy, which resulted in the complete breakage of the fibers in the transverse direction. Although the epoxy resin supported the specimen laminated at an angle of 0° in the transverse direction, the damage occurred due to the susceptibility of the resin to impacts.

The drop-weight impact test results of the specimens oriented at angles of 0°/90° and +45°/–45° exhibited that more than 90% of the impact energy applied by the impactor was not absorbed by the specimens, and was re-transferred to the impactor. The results can be attributed to the lamination of the fibers in orthogonal directions for both specimens.

The specimens after impact were analyzed using the lock-in method. The specimens were analyzed except the specimens laminated at an angle of 0° which underwent complete breakage during the impact test. The analysis results revealed that there was internal delamination and cut fibers, in addition to the visible damage. The finite element analysis showed that the damage of each fiber could be assessed and that the shape of damage was mainly dependent on the fibers orientation in the first half of the composite from the impactor side. But in the second haft, the damage in each ply was found to depend not only to the fiber orientation but also to the damage from the precedent ply which resulted in the more complex shape of the damage in the second half than in the first half of the composites. From the finite element analysis and non-destructive test, it was concluded that the image of whole composite damage obtained with lock-in testing was the combination of damage image of each ply. Moreover, it was found that from the simulation the critical orientation of damage propagation could be predicted. In the residual compression test results, the temperature differences were not significant, given that the already-impacted specimens were subjected to the compression test. The specimen laminated at angles of 0°/90° exhibited higher residual compressive strengths than that the composite laminated at +45°/–45°.

Author Contributions: Conceptualization, S.H.G and H.G.K; method, S.H.G and A.T, validation, S.H.G and H.G.K, writing-orginal draft preparation, S.H.G. and A.T., writing -review and editing, A.T., S.H.G., and H.G.K., supervision, H.G.K.; project administration, H.G.K.; funding acquisition, H.G.K.

.

Funding: This research was supported by Basic Science Research Program through the National Research Foundation of Korea (NRF) funded by the Ministry of Education (2016R1A6A1A03012069) and Korea government (MSIP) (No. 2017R1A2B4009646)

Acknowledgments: The authors thank the Korean Ministry of Education for funding this project and their co-workers for their supports.

Conflicts of Interest: There is no conflict of interest.

References

1. Kong, C.D.; Park, H.B.; Lim, S.J.; Shin, C.J. A study on compressive strength of carbon/epoxy composite structure repaired with bonded patches after impact damage. *Compos. Res.* **2010**, *23*, 15–21. https://doi.org/10.7234/kscm.2010.23.5.015.
2. Lee, J.H; Choi, S.W; Byun, J.H. A study on non-contacting ultrasonic testing for inspecting delamination in CFRP. *J. Kor. Soc. Precis. Eng.*, **2007**, *24*, pp. 23–30. https://doi.org/10.4028/0-87849-412-x.968.

3. Kim, W.T; Chio, M.Y.; Park, J.H. Analysis of thermal stress in fatigue fracture specimen using lock-in thermography. *Proceedings of the 2006 International Conference on Quantitative InfraRed Thermography (2006)*. https://doi.org/10.21611/qirt.2006.099
4. https://www.fibreglast.com/product/What-are-Unidirectional-Carbon-Fiber-Fabrics/Learning_Center, Availabe online, (Accessed on 30 October, 2020)
5. Daxi, G., Yihang, L., Zhenyu, S., Jun, C., Xun, L., Xinggang, J., Deyuan, Z. Delamination formation, evaluation and suppression during drilling of composite laminates. A review. *Compos. Struct*, ***2019***, *216, 168-186.*
6. Gholizadeh, S. A review of non-destructive testing methods of composite materials. *Procedia Struct. Integrity*, ***2016***, *1, 50-57*
7. Kim, K.S.; Jeon, S.Y.; Jung, H.C. Defect detection of impacted composite tubes by lock-in photo-infrared thermography technique. *J. Kor. Soc. Nondestruct. Test.*, **2011**, *31*, 139–143
8. Richardson, M.O.W.; Wisheart, M. Review of low-velocity impact properties for composite materials. *Composites, Part A* **1996**, *27*, pp. 1123–1131. https://doi.org/10.1016/1359-835x(96)00074-7
9. Serge, A. *Impact on Composite Structure*, Cambridge University Press, 1998.
10. Davies, G.A.O; Zhang, X. Impact damage prediction in carbon composite structures. *Int. J. Impact Eng.*, **1995**, *16*, 149–170. https://doi.org/10.1016/0734-743x(94)00039-y
11. Han, J.W. Low-velocity impact characterization of laminated composite materials. *KOSOS* **2008**, *23*, 24–27
12. Byun, J.I.; Kim, J.Y.; Heo, S.B.; Kim, H.S. Study on simulation characteristics of low velocity impact test of carbon/epoxy composites plates manufactured by filament winding method. *Trans. of Korean Hydrogen and New Energy Society*, **2018**, *29*, 190–196.
13. Go, S.H; Kim, H.G.; Shin, H.J; Lee, M.S.; Yoon, H.G.; Kwac, L.K. The impact fracture behaviors of CFRP/EVA composites by drop-weight impact test. *Carbon Lett.*, **2017**, *21*, 23–32. https://doi.org/10.5714/cl.2017.21.023.
14. Li, Y.; Zhang, W.; Yang, Z.W; Zhang, J.Y; Tao, S.J. Low-velocity impact damage characterization of carbon fiber reinforced polymer(CFRP) using infrared thermography. *Infrared Phys. Technol*., **2016**, *76*, 91–102. https://doi.org/10.1016/j.infrared.2016.01.019
15. Salvetti, M.; Gilioli, A.; Sbarufatti, C.; Dragan, K.; Chalimoniuk, M.; Manes, A.; Giglio, M. Analytical model to describe damage in CFRP specimen when subjected to low velocity impacts, *Procedia Eng*., **2016**, *167*, 2016, 2–9. https://doi.org/10.1016/j.proeng.2016.11.662
16. Kaybal, H.B.; Ulus, H.; Demir, O.; Sahin, O.S.; Avci, A. Effects of alumina nanoparticles on dynamic impact responses of carbon fiber reinforced epoxy matrix nanocomposites. *Eng. Sci. Technol. Int. J.*, **2018**, *21*, 399–407. https://doi.org/10.1016/j.jestch.2018.03.011
17. Daelemans, L.; Cohades, A.; Meireman, T.; Beckx, J.; Spronk, S.; Kersemans, M.; Baere, I.D.; Rahier, H.; Michaud, V.; Paepegem, W.V.; Clerck, K.D.; Electrospun nanofibrous interleaves for improved low velocity impact resistance of glass fibre reinforced composite laminates. *Mater. Des.*, **2018**, *141*, 170–184. https://doi.org/10.1016/j.matdes.2017.12.045
18. Li, Z.; Khennane, A.; Hazell, P.J.; Brown, A.D. Impact behaviour of pultruded GFRP composites under low-velocity impact loading. *Compos. Struct.*, **2017**, *168*, 360–371. https://doi.org/10.1016/j.compstruct.2017.02.073
19. Riccio, A.; Luca, A.D.; Felice, G.D.; Caputo, F. Modelling the simulation of impact induced damage onset and evolution in composites, *Composites: Part B*, **2014**, *66*, 340–347. https://doi.org/10.1016/j.compositesb.2014.05.024
20. Joo, H.J.; Son, J.S. The impact fracture behaviors of low density 2-D carbon/carbon composites by drop weight impact test. *Polymer (Korea)*, **2002**, *26*, pp. 270–278.
21. Kang, D.H.; Seo, M.Y.; Gimm, H.; Kim, T.W. Determination of shock absorption performance and shear modulus of rubbers by drop impact test, *Trans. Kor. Soc. Mech. Eng. A* **2009**, *33*, 321–328. https://doi.org/10.3795/ksme-a.2009.33.4.321
22. Suh, Y.W.; Woo, K.S.; Choi, I.H.; Kim, K.T.; Ahn, S.M. Analysis of low velocity impact damage and compressive strength after impact for laminated composites. *Kor. Aerosp. Res. Inst.* **2011**, *10*, 183–192.
23. Go, S.H.; Lee, M.S.; Hong C.G.; Kwac, L.K.; Kim, H.G. Correlation Between Drop Impact Energy and Residual Compressive Strength According to the Lamination of CFRP with EVA Sheets. Polymers 2020,12, 224. https://doi.org/10.3390/polym12010224

24. Remacha, M.; Sanchez-Saez, S.; Lopez, B.; Barbero, E. A new device for determining the compression after impact strength in thin laminates. *Compos. Struct*., **2015**, *127*, 99–107. https://doi.org/10.1016/j.compstruct.2015.02.079
25. Falaschetti, M.P; Scafe, M.; Troiani, E.; Agostinelli, V.; Sangiorgi, S. Experimental determination of compressive residual strength of a carbon/epoxy laminate after a near-edge impact. *Procedia Eng.* **2015**, *109*, 171–180. https://doi.org/10.1016/j.proeng.2015.06.229
26. Lopresto, V; Langella, A.; Papa, I. Residual strength evaluation after impact tests in extreme conditions on CFRP laminates. *Procedia Eng.* **2016**, *167*, 138–142. https://doi.org/10.1016/j.proeng.2016.11.680
27. Goo, J.S.; Shin, K.B.; Kim, J.S. Evaluation of impact damage and residual compression strength after impact of glass/epoxy laminate composites for lightweight bogie frame induced by ballast-flying phenomena. *J. Kor. Soc. Railw.* **2012**, *15*, 109–115. https://doi.org/10.7782/jksr.2012.15.2.109